Resistive-Pulse Sensing Inside Single Living Cells

Rongrong Pan,[†,§] Keke Hu,[†,‡] Rui Jia,[†,‡] Susan A. Rotenberg,[†,‡] Dechen Jiang,[§,*] and Michael V. Mirkin[†,‡,*]

[†] *Department of Chemistry and Biochemistry, Queens College-CUNY, Flushing, NY 11367, USA.*

[§] *State Key Laboratory of Analytical Chemistry for Life and School of Chemistry and Chemical Engineering, Nanjing University, Nanjing 210023, P. R. China*

[‡] *The Graduate Center of CUNY, New York, NY 10016.*

e-mail: mmirkin@qc.cuny.edu; dechenjiang@nju.edu.cn

ABSTRACT

Resistive-pulse sensing is a technique widely used to detect single nanoscopic entities such as nanoparticles and large molecules that can block the ion current flow through a nanopore or a nanopipette. Although the species of interest, e.g., antibodies, DNA, and biological vesicles, are typically produced by living cells, so far, they have only been detected in the bulk solution since no localized resistive-pulse sensing in biological systems has yet been reported. In this report, we used a nanopipette as a scanning ion conductance microscopy (SICM) tip to carry out resistive-pulse experiments both inside immobilized living cells and near their surfaces. The characteristic changes in the ion current occurring when the pipette punctures the cell membrane are used to monitor its insertion into the cell cytoplasm. Following the penetration, cellular vesicles (phagosomes, lysosomes, and/or phagolysosomes) were detected inside a RAW 264.7 macrophage. Much smaller pipettes were used to selectively detect 10 nm Au nanoparticles in the macrophage cytoplasm. The *in situ* resistive-pulse detection of extracellular vesicles released by metastatic human breast cells (MDA-MB-231) is also demonstrated. Electrochemical resistive-pulse experiments were carried out by inserting a conductive carbon nanopipette into a macrophage cell to sample single vesicles and measure reactive oxygen and nitrogen species (ROS/RNS) contained inside them.

INTRODUCTION

Direct detection, sampling and analysis of nanoscale objects in living cells, including nanoparticles (NP) and biological vesicles, are of great importance to several areas of biomedical research ranging from nanotoxicology, to neurochemistry, photodynamic therapy, and immunology.[1-3] A number of biologically important species are stored and released in biological vesicles, such as synaptic vesicles[4-6] and lysosomes.[7] Counting, sampling, and analyzing contents of individual vesicles inside the cell is a major challenge in bioanalytical chemistry.[4] Carbon nanofibers with a small tip radius[8,9] and platinized nano-disk electrodes[10] have recently been applied to electrochemical measurements of neurotransmitters and reactive oxygen/nitrogen species in single biological vesicles.[4,11] A somewhat related problem is the detection and analysis of extracellular vesicles[12] released from biological cells that have shown potential for cancer diagnostics.[13,14] Most reported efforts focused on measuring extracellular vesicles in blood and other body fluids,[15,16] although monitoring and sampling single vesicles secreted by a specific cell near its surface may be advantageous for research and diagnostics.

Florescence microscopy and related techniques have been widely employed for detecting and monitoring NPs in living cells.[17,18] It was noticed, however, that surface-bound fluorescent labels may affect native cellular recognition events.[19] Label-free optical techniques are typically suitable for the detection of relatively large nanoparticles. For instance, scatter enhanced phase contrast microscopy was used for monitoring the uptake and transport of metal and oxide NPs down to ~35 nm.[19] In situ TEM[20] and surface-enhanced Raman scattering[21] were used to image unlabeled gold nanorods inside various living cells.

Resistive-pulse sensing with biological or solid-state nanopores and nanopipettes—a powerful technique for detecting nanoscale objects, including single nanoparticles and vesicles—

relies on measurements of the ion current flowing through a nanopore.[22,23] A nanoparticle (NP)[22-24] or a vesicle,[25,26] entering the nanopore orifice affects its conductance, causing a transient decrease in the ion current (resistive pulse). Although detecting single nanoobjects in small spaces (e.g., inside living cells and their organelles) can be useful, all reported resistive-pulse experiments were carried out in bulk solution. Here we develop methodology for localized resistive-pulse sensing of vesicles and nanoparticles inside and near single biological cells.

Nanopipette-based resistive-pulse and electrochemical techniques provided several promising approaches to single-entity measurements.[26-31] A nanopipette possesses a small physical size (down to a few nm at the tip) and shape that makes it suitable as a scanning ion conductive microscopy (SICM) or scanning electrochemical microscopy (SECM) tip. In this way, a nanopipette can be inserted into a living cell or positioned close to its surface. The possibility of resistive-pulse experiments in a living cell is, however, counterintuitive because the ion current flowing through a nanopipette is very sensitive to the medium and often exhibits instabilities even in aqueous solutions with low level of impurities and no added surfactants. Plugging of the pipette orifice by lipids, proteins, and other biomolecules inside a cell may preclude meaningful resistive-pulse measurements. The present work not only showcases the possibility of localized resistive-pulse sensing in biological cells, but also demonstrates that nanopipettes with a wide range of radii can detect different kinds of nanoobjects inside living cells and near their surfaces.

We have recently introduced a new version of the resistive-pulse technique based on the use of conductive carbon nanopipettes (CNP), where the current produced by electrochemical oxidation/reduction of redox molecules at the carbon surface responds to the particle translocation.[32] In addition to counting single entities, this technique enables qualitative and

quantitative analysis of the electroactive material they contain. Here we insert a CNP inside a living macrophage cell by using it as a SECM tip and carry out electrochemical resistive-pulse experiments to measure reactive oxygen and nitrogen species (ROS/RNS) contained in macrophage vesicles. Four types of resistive-pulse experiments performed with either quartz nanopipettes or CNPs inside living cells are shown schematically in Fig. S1.

EXPERIMENTAL SECTION

Fabrication and characterization of quartz, carbon, and platinized carbon nanopipettes. Nanopipettes with the tip diameter from 25 nm to 400 nm are prepared by pulling quartz capillaries (1.0 mm o.d., 0.5 mm i.d.) with the laser pipette puller (P-2000, Sutter Instruments). A layer of carbon was deposited on the inner surface of the nanopipette by chemical vapor deposition (CVD) at 950 °C, using methane as carbon source and argon as protector (methane/argon: 5/3), as described previously.[33] The appropriate protection was used to avoid electrostatic damage to the nanotips.[34] The size and geometry of the tips were characterized by TEM (JEOL TEM-2100 Instrument) with a relatively low electron beam voltage of 80 kV used to avoid damage to the pipettes (Fig. S2).

Platinized CNP were produced by electrodepositing Pt onto the inner carbon wall at -80 mV vs. Ag/AgCl, as described previously.[10,32] Briefly, The platinizing solution contained 130 μL hexachloroplatinic acid (8 wt. %) and 0.216 mg lead(II) acetate trihydrate in 4.87 mL PBS (10 mM). The deposition was stopped after the current began to grow slowly but before the sharp increase in current.[32] A TEM image of a typical platinized CNP is shown in Fig. S2D .

Instrumentation and procedures. The SICM and SECM experiments with immobilized cells were performed inside a Faraday cage with a previously described home-built instrument[10,35] set on an optical table. A plastic 60-mm culture dish with cells was mounted on the horizontal stage of Axiovert-S100 microscope (Zeiss) that was set on the same optical table,

and the nanopipette tip was positioned directly above a single cell. SICM approach curves were obtained by slowly moving the quartz pipette tip vertically down to the cell surface (at 0.5 μm/s) and penetrating the cell. The voltage, $V = 0.4$ V was applied between the internal and external Ag/AgCl reference electrodes. After the nanopipette entered the cell, the approach was stopped and the applied voltage adjusted to the value required for resistive-pulse measurements. SECM approach curves were obtained similarly, except that a CNP (either bare or platinized) was used as a working electrode, and the tip current was produced by oxidation of the redox species (1 mM ferrocenemethanol (FcMeOH) and 10 mM $K_4[Fe(CN)_6]$) at the carbon surface near the orifice. The tip potential was sufficiently positive (0.4 V vs Ag/AgCl) for the SECM feedback to be governed by diffusion.

Resistive-pulse experiments were carried out with a patch clamp amplifier (Multiclamp 700B, Molecular Devices Corporation) coupled with the above SECM instrument in the voltage-clamp mode. The signal was digitized using a Digidata 1550A analog-to-digital converter (Molecular Devices) at a sampling frequency of 100 kHz and a 2 kHz low pass filter frequency. The data was analyzed using pClamp 10 software (Molecular Devices). 10 mM PBS with pH 7.4 (10 mM Na_2HPO_4, 2.7 mM KCl and 137 mM NaCl) was used in resistive-pulse sensing of cellular vesicles and EVs. The solution containing 10 mM PB, 10 mM KCl and 5% glucose was used in resistive-pulse sensing of 10 nm AuNPs.

AuNPs were characterized using dynamic light scattering (DLS). A Malvern Zetasizer, Nano-ZS (Malvern Instruments, UK) employing a 173° scattering angle and a 4 mW incident He−Ne laser (633 nm) was used to measure particle sizes (hydrodynamic diameter), size distributions, and zeta potentials at 25 °C.

RESULTS AND DISCUSSION

Controlled penetration of macrophage cells with quartz nanopipettes. A quartz nanopipette was inserted into an immobilized RAW 264.7 murine macrophage cell, as shown in Fig. 1. The voltage, $V = 0.4$ V was applied between the Ag/AgCl electrode inside the nanopipette and the Ag/AgCl electrode in the bulk solution. The nanopipette served as a SICM tip, and the measured ion current was inversely proportional to the resistance between the internal and external reference electrodes. When the nanopipette approached the cell surface, this resistance increased with decreasing separation distance between its orifice and the membrane.

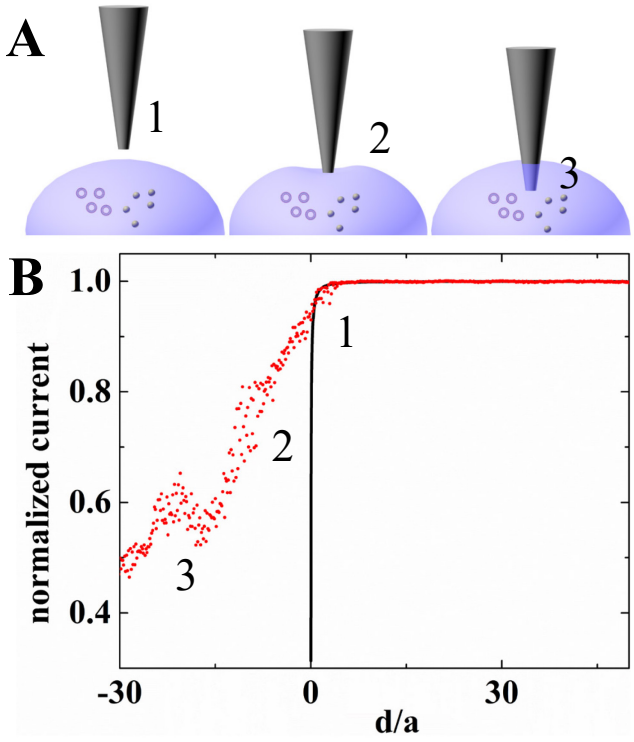

Fig. 1. Controlled cell penetration with a quartz nanopipette used as a SICM tip. (A) Schematic diagram of the pipette tip approaching the cell (1), pushing the membrane (2), and penetrating inside the cell (3). (B) SICM approach curve obtained with a 150 nm diameter nanopipette approaching an immobilized RAW 264.7 macrophage in 10 mM PBS solution. The experimental data (symbols) are fitted to the theory for negative SICM feedback (solid line [35]). The approach velocity was 0.5 μm/s. $V = 0.4$ V.

The SICM current vs. distance curve includes three distinct regions shown schematically in Fig. 1A and labeled by corresponding numbers in Fig. 1B. The ion current (i) is essentially independent of the pipette tip position until the distance between the orifice and cell membrane (d) becomes comparable to the pipette radius (a) (region 1). The experimental $i - d$ curve initially fits the theory (solid line calculated from Eq. (1) in ref. 35) and deviates from it when the pipette tip begins to push the cell membrane (region 2; positive d corresponds to the tip approaching the membrane; negative distances correspond to the tip pushing the membrane and then penetrating the cell). When the tip punctures a hole in the cell membrane, the resistance between the internal and external reference electrodes decreases abruptly, causing a sudden increase in the measured current ($d/a \approx -19$; Fig. 1B). This feature, which was reproducibly observed with a number of different pipettes and cells, corresponds to the moment when the tip penetrates the cell membrane and enters its cytoplasm. The subsequent slower decrease in the current is due to the membrane sealing around the wall of the pipette (region 3). After the penetration was detected, the pipette was stopped, and resistive-pulse recordings were obtained. (If the pipette continues to travel downward, the current eventually decreases to zero when its orifice reaches the bottom of the cell; data not shown). Somewhat similar approach curves were obtained previously for a metal SECM tip penetrating a macrophage, but the change in the current was due to impermeability of the membrane to the redox mediator species (see below).[10]

Resistive-pulse sensing of vesicles inside a macrophage cell. A resistive-pulse recording in Fig. 2A obtained with a 140-nm-diameter quartz pipette inside a macrophage at $V = 0.4$ V shows a large number of current blockages. Macrophages are known to contain different biological vesicles (lysosomes, phagosomes, phagolysosomes) whose size may vary from nanometers to micrometers.[7,10,36] Accordingly, the scatter plot in Fig. 2B shows a wide

range of translocation time values (τ, i.e. the width at half peak height) *ca.* 3 - 10 ms and a very broad distribution of the resistive-pulse amplitude (Δi_{max}) from <1% of the base current (i_0) to almost complete current blockages. This $\Delta i_{max}/i_o$ range corresponds to the vesicle diameters from 40-50 nm to ~140 nm.[37,38] Although larger vesicles may have been present inside the macrophage, they could not translocate through the pipette. It was shown recently that liposomes with a diameter significantly larger than that of the pipette orifice do not produce measurable resistive pulses.[32] To check for the presence of smaller vesicles, controlled experiments were carried out with much smaller pipettes (e.g., 32 nm diameter; Fig. S3). No resistive pulses were recorded with this nanopipette (and similarly sized pipettes; not shown), suggesting that phagosomes and other vesicles in a macrophage cell are larger than ~30 nm. No current spikes were also observed outside of the macrophage cell either before the pipette insertion (Fig. S3A) or after its withdrawal from the cell (Fig. S3C).

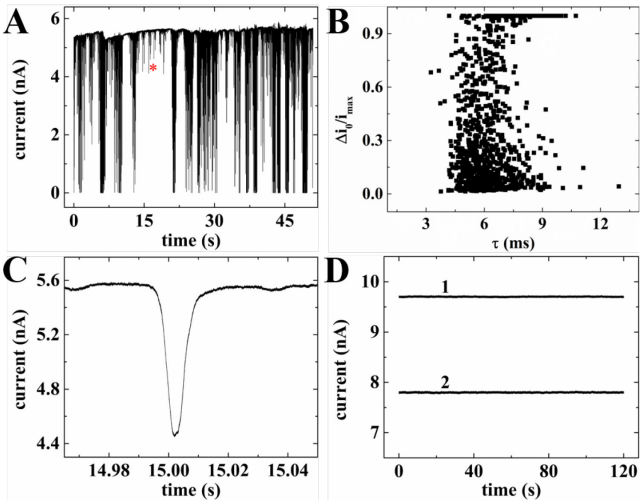

Fig. 2. Resistive-pulse sensing of cellular vesicles within a RAW 264.7 macrophage cell with a 140-nm-diameter quartz pipette. (A) Current-time recording with the nanopipette inside the cell. (B) Scatter plot of the normalized maximum current change vs. peak width for transients shown in A. (C) Blowup of the transient labeled by the red asterisk in A. (D) Current-time recordings obtained with the same nanopipette before its insertion into the cell (curve 1) and after the withdrawal from the cell (curve 2). $V = 0.4$ V.

A typical translocation transient (Fig. 2C) is an asymmetrical peak with the sharp initial decrease in current followed by a longer tail.[22,28] While the shape of the peak is similar to those measured recently with liposomes in aqueous solutions, the mean translocation time (τ = 6.2 ms) is much longer than $\tau \leq 1.5$ ms obtained in those experiments.[32] The difference may be due to significantly slower diffusion in more viscous and crowded cytoplasm than in water and vesicle interactions with biological structures inside the cell.[39] The average translocation frequency is 22.4 s^{-1} for the 5 min recording. No resistive pulses were recoded with the same nanopipette positioned near the cell surface either before its insertion into the cell (curve 1 in Fig. 2D) or after the withdrawal (curve 2 in Fig. 2D). The base current in curve 2 is higher than that measured inside the cell (*cf.* Fig. 2A) but ~20% lower than that in curve 1, indicating that some material from the cytoplasm entered the pipette during the intracellular measurements.

In a conceptually similar experiment, a CNP was employed for resistive-pulse sensing of vesicles in a macrophage (Fig. S1B). A current-time recording obtained in such an experiment is shown in Fig. S4A. The inner surface of quartz pipettes and CNPs is negatively charged,[40] and so the duration of resistive pulses obtained with CNPs (Fig. S4B) and the shape of a typical translocation transient (Fig. S4C) are comparable to those measured with a similarly sized quartz pipette. No currents spikes were obtained outside of the cell before the CNP insertion (curve 1 in Fig. S4D) and after its withdrawal from the cell (curve 2 in Fig. S4D). The use of CNPs is essential for electrochemical resistive-pulse sensing in macrophages (see below).

Resistive-pulse sensing of Au nanoparticles (AuNPs) inside a macrophage cell. The data in Fig. S3 shows that no mobile nanoscale objects in the cytoplasm of a macrophage cell possess the right size (i.e., ~10 - 30 nm diameter) to produce resistive-pulse signal measurable with *ca.* 30-nm-diameter pipettes. Thus, it may be possible to use such a pipette to detect

nanoparticles pre-accumulated within the cell. We employed as a model system commercial citrate-stabilized 10 nm AuNPs that have previously been detected in resistive-pulse experiments with quartz nanopipettes.[38,41] The total electrolyte concentration in refs. 38 and 41 was *ca.* 10-20 mM because AuNPs may aggregate at a significantly higher ionic strength. The electrolyte concentration in experiments with living cells is typically much higher because of the cell-solution osmotic equilibration. The effective diameter of AuNPs either in water or in 10 mM PB containing 10 mM KCl was ~20 nm from DLS measurements (Table S1), i.e. about twice the 10 nm nominal AuNP diameter confirmed by TEM (Fig. S5). Both numbers are in close agreement with the previous report,[41] where DLS was found to significantly overestimate the mean NP size. However, the apparent AuNP diameter measured by DLS in 10 mM PBS containing 0.137 mM NaCl (612 ± 21 nm; Table S1) points to extensive NP aggregation.

The pH 7.4 solution containing 10 mM PB, 10 mM KCl and 5% glucose is essentially isotonic with the cell cytoplasm without causing significant AuNP aggregation (the mean NP diameter measured by DLS is 17.7 ± 0.4 nm; Table S1). Well-defined resistive pulses of translocations of 10 nm AuNPs through a 30 nm quartz nanopipette recorded in this solution are shown in Fig. S6A. The related scatter plot (Fig. S6B) and the shape of a representative current spike (Fig. S6C) are similar to those reported previously.[38] By contrast, the current–time recordings obtained with 0.47 nM AuNPs in 10 mM PBS solution exhibit no resistive pulses (Fig. S6D).

For intracellular detection of NPs, adherent RAW246.7 macrophage cells were incubated with 10 nm AuNPs for 4 h,[42] washed three times with buffer, and then transferred to fresh buffer solution of the same composition for resistive-pulse experiments. The current-time recording (Fig. 3A) shows translocations of 10 nm AuNPs through the 30 nm pipette inside the cell driven

by positive voltage (0.4 V vs. external Ag/AgCl reference). No resistive-pulse spikes were obtained with a negative voltage, -0.4 V, applied to the pipette. The scatter plot for AuNP translocations (Fig. 3B) and a typical current spike (Fig. 3C) show that the current blockages inside a cell are significantly longer than those recorded in solution (τ = 4.8 ms vs. 0.5 ms in Fig. S6). The likely reasons for this difference are the slower mobility of AuNPs due to the more viscous cytoplasmic environment and adsorption of biomolecules on the nanoparticle surface. Importantly, the absence of spikes in current recordings obtained with the same nanopipette positioned near the cell surface either before entering (curve 1 in Fig. 3D) or after withdrawing from the macrophage (curve 2 in Fig. 3D) suggest that only AuNPs accumulated inside the cell are detected by localized resistive-pulse measurements.

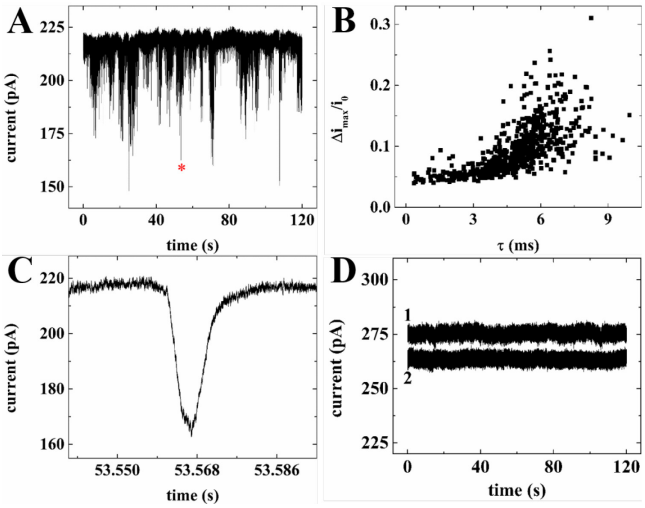

Fig. 3. Resistive-pulse sensing of 10 nm AuNPs in a RAW 264.7 macrophage cell. Current-time recordings were obtained with a 30 nm quartz nanopipette at V = 0.4 V (A) inside the cell and (D) near the cell surface before penetration (curve 1) and after withdrawal from the macrophage (curve 2). (B) Scatter plot of the normalized maximum current change vs. peak width for transients shown in A. (C) Individual resistive-pulse spike labeled with the red asterisk in A. Solution contained 10 mM PB, 10 mM KCl and 5% glucose.

In agreement with an earlier report,[42] the mean frequency of translocations measured inside a macrophage incubated with 10 nm AuNP for 4 h (15.6 ± 6.7 s^{-1}; 500 s recording time, six cells) is higher than the frequency measured after the 30-min-long incubation (7.7 ± 3.6 s^{-1}; 500 s recording time, three cells). This proof-of-concept experiment suggests the possibility of studying kinetics of NP endocytosis by resistive-pulse techniques.

Electrochemical resistive-pulse sensing of vesicles inside a macrophage cell. An experiment employing a CNP for electrochemical resistive-pulse sensing of cellular vesicles inside a macrophage is shown schematically in Fig. S1C. In these experiments the CNP serves as a working electrode, and the measured current is due to the diffusion of the redox species to the pipette orifice and their oxidation at the carbon surface. To insert the CNP into a macrophage, it was used as an SECM tip (Fig. S7A). 10 mM PBS solution contained two redox mediators, 1 mM FcMeOH and 10 mM $K_4[Fe(CN)_6]$. When the tip approached an immobilized macrophage, hydrophilic $Fe(CN)_6^{4-}$ species that could not cross the cell membrane produced negative SECM feedback response, enabling precise monitoring of the membrane penetration.[10,43] The oxidation of hydrophobic FcMeOH at the CNP produced the base faradaic current for electrochemical resistive-pulse sensing inside the cell. A current-time recording for vesicle translocations through the CNP (Fig. S7B) and the shape of a representative current transient (Fig. S7C) are similar to those obtained with quartz nanopipettes (Fig. 2). It was shown in ref. 32 that electrochemical resistive-pulse experiments can be performed with no redox species added to solution by using oxygen reduction at the CNP as the source of current. This approach can be used for intracellular experiments (data not shown), but the detection of the cell penetration by CNP is harder without a redox mediator.

We used platinized CNPs[44] (Fig. S2D) to combine electrochemical resistive-pulse sensing with electroanalysis of single vesicle contents (Fig. S1D). Unlike experiments performed with an unmodified CNP (Fig. S7), both downward and upward spikes can be seen in the current-time recording obtained with a platinized CNP inside a macrophage cell (Fig. 4A). The current blockages produced by vesicle translocations are similar to the resistive pulses in Fig. S7 (cf. Figs. 4B and S7C). The current upsurges (Figs. 4A and 4C) are caused by oxidation of ROS/RNS contained in the vesicles during their collisions with the carbon surface. These transients are only produced by vesicles entering the CNP rather than by blockages of the CNP orifice from the cytoplasm side or collisions of vesicles with the carbon ring exposed to the cytoplasm.[32] (The recordings obtained with pipettes whose orifice diameters were smaller than that of the vesicles showed no current spikes; see Fig. S3 and also Fig. S4 in ref. 32).

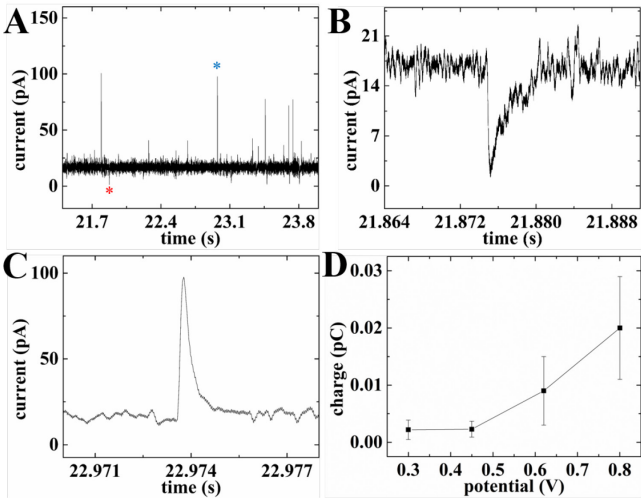

Fig. 4. Electrochemical resistive-pulse sensing of ROS/RNS inside cellular vesicles within a RAW 264.7 macrophage cell. (A) Current-time recording obtained with a 210 nm platinized CNP. (B) Individual resistive-pulse spike labeled with a red asterisk in A. (C) Representative vesicle collision transient labeled with a blue asterisk in A. CNP potential was 0.8 V vs. Ag/AgCl. (D) Dependence of the mean vesicle collision charge on CNP potential. 10 mM PBS solution contained 1 mM FcMeOH and 10 mM $K_4[Fe(CN)_6]$.

All four primary ROS/RNS produced in macrophages (i.e. H_2O_2, $ONOO^-$, $NO^\bullet$ and NO_2^-) get oxidized at platinized CNPs biased at 0.8 V vs. Ag/AgCl.[10] Unlike ref. 10, where measurements performed with a nanoelectrode inserted inside a phagolysosome characterized the production rate of ROS/RNS on the long experimental time scale (minutes), the integration of the current under each spike in Fig. 4A yields the charge corresponding to the total amount of ROS/RNS oxidized during a specific collision. To estimate contributions of individual ROS/RNS to the measured charge, the current-time recordings were obtained with the same platinized CNP biased at different potentials. The potential program developed by the Amatore group consisted of four potential steps roughly corresponding to the oxidation of H_2O_2 (300 mV vs. Ag/AgCl), H_2O_2 and $ONOO^-$ (450 mV), H_2O_2, $ONOO^-$ and $NO^\bullet$ (620 mV), and all four species (800 mV).[45] The average values of charge passed during a single vesicle collision (Fig. 4D) were calculated from current-time recordings obtained with the same platinized CNP at these potential values (Fig. 4A and Fig. S8). With the number of transferred electrons, $n_{H_2O_2}$ = $n_{NO_2^-}$ = 2 and n_{ONOO^-} = n_{NO} = 1, the corresponding amounts of ROS/RNS in a vesicle (pmol) are: 1.1×10^{-8} (H_2O_2), 1×10^{-9} ($ONOO^-$; this number is too low for reliable analytical determination), 6.7×10^{-8} ($NO^\bullet$), and 1.1×10^{-7} (NO_2^-). Very small amounts of hydrogen peroxide and peroxynitrite (as compared to $NO^\bullet$ and NO_2^-) contained in a vesicle may be related to low production rates of these species reported earlier,[10] but direct comparison may not be meaningful because the experiments in ref. 10 were done with immunostimulated macrophages. (The total ROS/RNS contents of individual phagolysosomes in resting and activated macrophages were recently evaluated.[11]) Interestingly, the vesicle collision frequency was much lower when the CNP potential was 450 mM or 300 mV (Figs. S8B and S8C) than at 620 mV or 800 mV (Figs. S8A and 4A). Apparently, among the heterogeneous population of vesicles probed in our

experiments, a larger fraction contains NO_2^- and/or $NO^\bullet$ species than H_2O_2 and $ONOO^-$. Additional experiments are needed to clarify this issue.

Resistive-pulse sensing of extracellular vesicles (EVs) released by single breast cancer cells. Extracellular vesicles released from breast cancer cells, including metastatic MDA-MB-231 human breast cells, have been studied previously.[46,47] To explore the possibility of resistive-pulse sensing of EVs, a 300 nm diameter quartz pipette was used as an SICM tip and positioned near the surface of an MDA-MB-231 cell (Fig. 5A). Unlike the above intracellular measurements, our goal here was not to penetrate the cell but to avoid touching its membrane. Thus, the approach in Fig. 5A was stopped when the current decreased by only ~5%, and the pipette tip was relatively far from the cell top. One should notice that the diffusion time for nm-sized vesicle crossing a sub-micrometer cell/nanopipette gap is on the millisecond time scale, allowing us to monitor the EV release in real time.

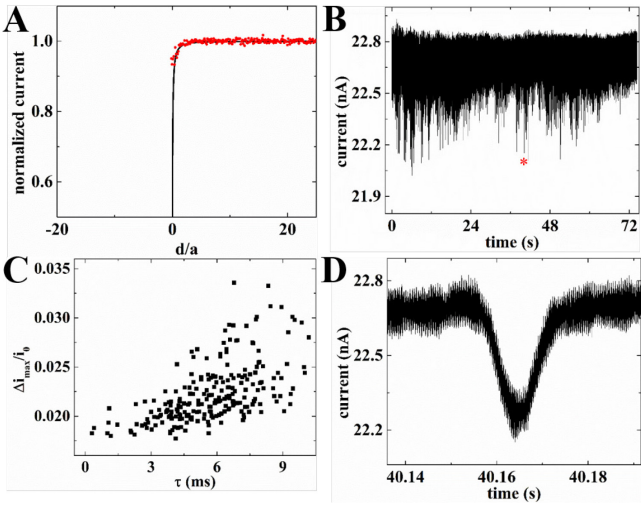

Fig. 5. Resistive-pulse monitoring of EVs released by a single MDA-MB-231 cell. (A) SICM approach curve obtained during the positioning of a 300 nm quartz nanopipette above an immobilized MDA-MB-231 cell in 10 mM PBS. The approach velocity was 0.4 μm/s. (B) Current-time recording obtained with the same nanopipette. (C) Scatter plot of the normalized maximum current change vs. peak width for transients shown in B. (D) Individual resistive pulse labeled with the red asterisk in B. $V = 0.4$ V.

The translocation transients of EVs released by a single living MDA-MB-231 cell are shown in Fig. 5B. The average frequency of EV translocations, 0.4 s^{-1} (total recording time, 9.2 min), is significantly lower than that found for intracellular vesicles in Fig. 2. Fig. 5C shows a scatter plot of EVs translocations, and a typical translocation transient is shown in Fig. 5D. The mean pulse width (τ = 5.7 ms) is only slightly shorter than that for vesicle translocations monitored inside macrophage cells (6.2 ms). No resistive-pulse spikes were recorded with the nanopipette far away from the cell. *In situ* detecting extracellular vesicles produced by a specific cell, evaluating their size, and analyzing their contents is potentially useful for diagnostic applications and for investigating possible role of such vesicles in cell signaling.[48]

CONCLUSIONS

Localized resistive-pulse sensing inside biological cells and near their surfaces is a powerful tool for the detection and analysis of nanoscale objects, such as vesicles and nanoparticles, in biological systems. Early resistive-pulse experiments employed biological and synthetic nanopores that combine very small size of the sensing element with much larger physical dimensions of the device, making this technique most suitable for measurements in the bulk solution.[22,23] By contrast, quartz and carbon nanopipettes employed in this study can be inserted into biological cells (and subcellular compartments[10]) and used to monitor processes involving vesicles and NPs in real time. The orifice diameter can be varied to match the size of a specific entity for selective and sensitive detection. In this way, cellular vesicles and EVs released by breast cancer cells were detected with relatively large quartz pipettes, and much smaller pipettes were used to monitor the uptake of 10 nm AuNPs by macrophages.

Recently developed electrochemical resistive-pulse technique employing CNPs was shown to be suitable for intracellular sensing. A platinized CNP was used as an electrochemical

nanosensor to selectively measure four ROS/RNS inside single vesicles within the macrophage. This approach is potentially useful for sampling and analyzing physiologically important species in subcellular compartments such lysosomes[31] and synaptic vesicles.[4]

Supporting Information. Supplementary materials and methods, additional resistive-pulse recordings, and TEM images of CNPs and NPs, including Figures S1 – S8 and Table S1. This material is available free of charge via the Internet at http://pubs.acs.org.

ACKNOWLEDGMENTS

The support of this work by the National Science Foundation (CHE-1763337; MVM) and by Ministry of Science and Technology of China (2017YFA0700500; DJ and RP) is gratefully acknowledged. RP thanks China Scholarship Council for a scholarship. We thank Prof. Uri Samuni and Dr. Jorge Ramos for assistance with DLS experiments and Dr. Je Hyun Bae for helpful discussions.

COMPETING INTERESTS STATEMENT

The authors declare that they have no conflict of interest.

References

(1) Chinen, A. B.; Guan, C. M.; Ferrer, J. R.; Barnaby, S. N.; Merkel, T. J.; Mirkin, C. A. Nanoparticle probes for the detection of cancer biomarkers, cells, and tissues by fluorescence. *Chem. Rev.* **2015,** *115*, 10530-10574.

(2) Doane, T. L.; Burda, C. The unique role of nanoparticles in nanomedicine: imaging, drug delivery and therapy. *Chem. Soc. Rev.* **2012,** *41*, 2885-2911.

(3) Grant, B. D.; Donaldson, J. G. Pathways and mechanisms of endocytic recycling. *Nat. Rev. Mol. Cell Biol.* **2009,** *10*, 597-608.

(4) Phan, N. T.; Li, X.; Ewing, A. G. Measuring synaptic vesicles using cellular electrochemistry and nanoscale molecular imaging. *Nat. Rev. Chem.* **2017,** *1*, 1-18.

(5) De Toledo, G. A.; Fernandez-Chacon, R.; Fernandez, J. M. Release of secretory products during transient vesicle fusion. *Nature* **1993,** *363*, 554-558.

(6) Stevens, C. F. Neurotransmitter release at central synapses. *Neuron* **2003,** *40*, 381-388.

(7) Gordon, S. Phagocytosis: an immunobiologic process. *Immunity* **2016,** *44*, 463-475.

(8) Li, X.; Majdi, S.; Dunevall, J.; Fathali, H.; Ewing, A. G. Quantitative measurement of transmitters in individual vesicles in the cytoplasm of single cells with nanotip electrodes. *Angew. Chem. Int. Ed.* **2015,** *54*, 11978-11982.

(9) Li, Y. T.; Zhang, S. H.; Wang, L.; Xiao, R. R.; Liu, W.; Zhang, X. W.; Zhou, Z.; Amatore, C.; Huang, W. H. Nanoelectrode for amperometric monitoring of individual vesicular exocytosis inside single synapses. *Angew. Chem. Int. Ed.* **2014,** *53*, 12456-12460.

(10) Hu, K.; Li, Y.; Rotenberg, S. A.; Amatore, C.; Mirkin, M. V. Electrochemical measurements of reactive oxygen and nitrogen species inside single phagolysosomes of living macrophages. *J. Am. Chem. Soc.* **2019,** *141*, 4564-4568.

(11) Zhang, X. W.; Oleinick, A.; Jiang, H.; Liao, Q. L.; Qiu, Q. F.; Svir, I.; Liu, Y. L.; Amatore, C.; Huang, W. H. Electrochemical monitoring of ROS/RNS homeostasis within individual phagolysosomes inside single macrophages. *Angew. Chem. Int. Ed.* **2019,** *58*, 7753-7756.

(12) Colombo, M.; Raposo, G.; Théry, C. Biogenesis, secretion, and intercellular interactions of exosomes and other extracellular vesicles. *Annu. Rev. Cell. Dev. Biol.* **2014,** *30*, 255-289.

(13) Sheridan, C. Exosome cancer diagnostic reaches market. *Nat. Biotechnol.* **2016,** *34*, 359-360.

(14) Zhu, Y.; Pick, H.; Gasilova, N.; Li, X.; Lin, T.-E.; Laeubli, H. P.; Zippelius, A.; Ho, P.-C.; Girault, H. H. MALDI detection of exosomes: a potential tool for cancer studies. *Chem* **2019,** *5*, 1318-1336.

(15) Yoshioka, Y.; Kosaka, N.; Konishi, Y.; Ohta, H.; Okamoto, H.; Sonoda, H.; Nonaka, R.; Yamamoto, H.; Ishii, H.; Mori, M. Ultra-sensitive liquid biopsy of circulating extracellular vesicles using ExoScreen. *Nat. Commun.* **2014,** *5*, 3591-3598.

(16) Shao, H.; Im, H.; Castro, C. M.; Breakefield, X.; Weissleder, R.; Lee, H. New technologies for analysis of extracellular vesicles. *Chem. Rev.* **2018,** *118*, 1917-1950.

(17) Chen, S.; Wang, J.; Xin, B.; Yang, Y.; Ma, Y.; Zhou, Y.; Yuan, L.; Huang, Z.; Yuan, Q. Direct observation of nanoparticles within cells at subcellular levels by super-resolution fluorescence imaging. *Anal. Chem.* **2019,** *91*, 5747-5752.

(18) Gao, Y.; Yu, Y. Macrophage uptake of Janus particles depends upon Janus balance. *Langmuir* **2015,** *31*, 2833-2838.

(19) Zimmerman, J. F.; Ardoña, H. A. M.; Pyrgiotakis, G.; Dong, J.; Moudgil, B.; Demokritou, P.; Parker, K. K. Scatter enhanced phase contrast microscopy for discriminating mechanisms of active nanoparticle transport in living cells. *Nano Lett.* **2019,** *19*, 793-804.

(20) Pohlmann, E. S.; Patel, K.; Guo, S.; Dukes, M. J.; Sheng, Z.; Kelly, D. F. Real-time visualization of nanoparticles interacting with glioblastoma stem cells. *Nano Lett.* **2015,** *15*, 2329-2335.

(21) Huang, J.-A.; Caprettini, V.; Zhao, Y.; Melle, G.; Maccaferri, N.; Deleye, L.; Zambrana-Puyalto, X.; Ardini, M.; Tantussi, F.; Dipalo, M. On-demand intracellular delivery of single particles in single cells by 3D hollow nanoelectrodes. *Nano Lett.* **2019,** *19*, 722-731.

(22) Bayley, H.; Martin, C. R. Resistive-pulse sensing from microbes to molecules. *Chem. Rev.* **2000,** *100*, 2575-2594.

(23) Shi, W.; Friedman, A. K.; Baker, L. A. Nanopore sensing. *Anal. Chem.* **2017,** *89*, 157-188.

(24) Luo, L.; German, S. R.; Lan, W.-J.; Holden, D. A.; Mega, T. L.; White, H. S. Resistive-pulse analysis of nanoparticles. *Annu. Rev. Anal. Chem.* **2014,** *7*, 513-535.

(25) Chen, L.; He, H.; Jin, Y. Counting and dynamic studies of the small unilamellar phospholipid vesicle translocation with single conical glass nanopores. *Anal. Chem.* **2015,** *87*, 522-529.

(26) Liu, Y.; Xu, C.; Chen, X.; Wang, J.; Yu, P.; Mao, L. Voltage-driven counting of phospholipid vesicles with nanopipettes by resistive-pulse principle. *Electrochem. Commun.* **2018,** *89*, 38-42.

(27) Morris, C. A.; Friedman, A. K.; Baker, L. A. Applications of nanopipettes in the analytical sciences. *Analyst* **2010,** *135*, 2190-2202.

(28) Wang, Y.; Wang, D.; Mirkin, M. V. Resistive-pulse and rectification sensing with glass and carbon nanopipettes. *Proc. R. Soc. London Ser. A* **2017,** *473*, 20160931.

(29) Zhang, S.; Li, M.; Su, B.; Shao, Y. Fabrication and use of nanopipettes in chemical analysis. *Annu. Rev. Anal. Chem.* **2018,** *11*, 265-286.

(30) Yu, R. J.; Ying, Y. L.; Gao, R.; Long, Y. T. Confined Nanopipette Sensing: From Single Molecules, Single Nanoparticles, to Single Cells. *Angew. Chem. Int. Ed.* **2019,** *58*, 3706-3714.

(31) Pan, R.; Xu, M.; Burgess, J. D.; Jiang, D.; Chen, H.-Y. Direct electrochemical observation of glucosidase activity in isolated single lysosomes from a living cell. *Proc. Natl. Acad. Sci. U.S.A.* **2018,** *115*, 4087-4092.

(32) Pan, R.; Hu, K.; Jiang, D.; Samuni, U.; Mirkin, M. V. Electrochemical Resistive-Pulse Sensing. *J. Am. Chem. Soc.* ***2019****, 141, 19555-19559.*

(33) Hu, K.; Wang, Y.; Cai, H.; Mirkin, M. V.; Gao, Y.; Friedman, G.; Gogotsi, Y. Open carbon nanopipettes as resistive-pulse sensors, rectification sensors, and electrochemical nanoprobes. *Anal. Chem.* **2014,** *86*, 8897-8901.

(34) Nioradze, N.; Chen, R.; Kim, J.; Shen, M.; Santhosh, P.; Amemiya, S. Origins of nanoscale damage to glass-sealed platinum electrodes with submicrometer and nanometer size. *Anal. Chem.* **2013,** *85*, 6198-6202.

(35) Wang, Y.; Cai, H.; Mirkin, M. V. Delivery of single nanoparticles from nanopipettes under resistive‐pulse control. *ChemElectroChem* **2015,** *2*, 343-347.

(36) Russell, D. G.; VanderVen, B. C.; Glennie, S.; Mwandumba, H.; Heyderman, R. S. The macrophage marches on its phagosome: dynamic assays of phagosome function. *Nat. Rev. Immunol.* **2009,** *9*, 594-600.

(37) Heins, E. A.; Siwy, Z. S.; Baker, L. A.; Martin, C. R. Detecting single porphyrin molecules in a conically shaped synthetic nanopore. *Nano Lett.* **2005,** *5*, 1824-1829.

(38) Wang, Y.; Kececi, K.; Mirkin, M. V.; Mani, V.; Sardesai, N.; Rusling, J. F. Resistive-pulse measurements with nanopipettes: detection of Au nanoparticles and nanoparticle-bound anti-peanut IgY. *Chem. Sci.* **2013,** *4*, 655-663.

(39) Swaminathan, R.; Hoang, C. P.; Verkman, A. Photobleaching recovery and anisotropy decay of green fluorescent protein GFP-S65T in solution and cells: cytoplasmic viscosity probed by green fluorescent protein translational and rotational diffusion. *Biophys. J.* **1997,** *72*, 1900-1907.

(40) Wang, D.; Mirkin, M. V. Electron-transfer gated ion transport in carbon nanopipets. *J. Am. Chem. Soc.* **2017,** *139*, 11654-11657.

(41) Cai, H.; Wang, Y.; Yu, Y.; Mirkin, M. V.; Bhakta, S.; Bishop, G. W.; Joshi, A. A.; Rusling, J. F. Resistive-pulse measurements with nanopipettes: detection of vascular endothelial growth factor C (VEGF-C) using antibody-decorated nanoparticles. *Anal. Chem.* **2015,** *87*, 6403-6410.

(42) Bancos, S.; Tyner, K. M. Evaluating the effect of assay preparation on the uptake of gold nanoparticles by RAW264. 7 cells. *J. Nanobiotechnol.* **2014,** *12*, 45-56.

(43) Sun, P.; Laforge, F. O.; Abeyweera, T. P.; Rotenberg, S. A.; Carpino, J.; Mirkin, M. V. Nanoelectrochemistry of mammalian cells. *Proc. Natl. Acad. Sci. U.S.A.* **2008,** *105*, 443-448.

(44) Hu, K.; Gao, Y.; Wang, Y.; Yu, Y.; Zhao, X.; Rotenberg, S. A.; Gökmeşe, E.; Mirkin, M. V.; Friedman, G.; Gogotsi, Y. Platinized carbon nanoelectrodes as potentiometric and amperometric SECM probes. *J. Solid State Electrochem.* **2013,** *17*, 2971-2977.

(45) Amatore, C.; Arbault, S. p.; Koh, A. C. Simultaneous detection of reactive oxygen and nitrogen species released by a single macrophage by triple potential-step chronoamperometry. *Anal. Chem.* **2010,** *82*, 1411-1419.

(46) Kruger, S.; Elmageed, Z. Y. A.; Hawke, D. H.; Wörner, P. M.; Jansen, D. A.; Abdel-Mageed, A. B.; Alt, E. U.; Izadpanah, R. Molecular characterization of exosome-like vesicles from breast cancer cells. *BMC Cancer* **2014,** *14*, 44.

(47) Hattori, Y.; Shimada, T.; Yasui, T.; Kaji, N.; Baba, Y. Micro-and Nanopillar Chips for Continuous Separation of Extracellular Vesicles. *Anal. Chem.* **2019**, *91*, 6514-6521.

(48) Raposo, G.; Stahl, P. D. Extracellular vesicles: a new communication paradigm? *Nat. Rev. Mol. Cell Biol.* **2019,** *20*, 509-510.

For TOC only

Resistive pulse sensing and ROS/RNS analysis in living cells